Available online at www.sciencedirect.com
ScienceDirect
Journal of Magnetic Resonance 189 (2007) 209–216
JMR Journal of Magnetic Resonance
www.elsevier.com/locate/jmr

Sensitivity enhancement using paramagnetic relaxation in MAS solid-state NMR of perdeuterated proteins

Rasmus Linser [a], Veniamin Chevelkov [a], Anne Diehl [a], Bernd Reif [a,b,*]

[a] Leibniz-Institut für Molekulare Pharmakologie (FMP), Robert-Rössle Str. 10, 13125 Berlin, Germany
[b] Charité Universitätsmedizin, D-10115 Berlin, Germany

Received 1 July 2007; revised 6 September 2007
Available online 18 September 2007

Abstract

Previously, Ishii et al., could show that chelated paramagnetic ions can be employed to significantly decrease the recycle delay of a MAS solid-state NMR experiment [N.P. Wickramasinghe, M. Kotecha, A. Samoson, J. Past, Y. Ishii, Sensitivity enhancement in C-13 solid-state NMR of protein microcrystals by use of paramagnetic metal ions for optimizing H-1 T-1 relaxation, J. Magn. Reson. 184 (2007) 350–356]. Application of the method is limited to very robust samples, for which sample stability is not compromised by RF induced heating. In addition, probe integrity might be perturbed in standard MAS PRE experiments due to the use of very short duty cycles. We show that these deleterious effects can be avoided if perdeuterated proteins are employed that have been re-crystallized from D_2O:H_2O = 9:1 containing buffer solutions. The experiments are demonstrated using the SH3 domain of chicken α-spectrin as a model system. The labeling scheme allows to record proton detected ^1H, ^{15}N correlation spectra with very high resolution in the absence of heteronuclear dipolar decoupling. Cu–edta as a doping reagent yields a reduction of the recycle delay by up to a factor of 15. In particular, we find that the ^1H T_1 for the bulk H^N magnetization is reduced from 4.4 s to 0.3 s if the Cu–edta concentration is increased from 0 mM to 250 mM. Possible perturbations like chemical shift changes or line broadening due to the paramagnetic chelate complex are minimal. No degradation of our samples was observed in the course of the experiments.

Keywords: Deuteration; Paramagnetic relaxation enhancement; Micro-crystals; MAS solid-state NMR; Magic angle spinning

1. Introduction

MAS solid-state NMR on uniformly isotopically enriched proteins evolved rapidly in the last few years as a method for the determination of the structure [2,3] and for the characterization of dynamics [4–6] of biomolecules. The number of applications to more interesting samples, like, e.g. membrane proteins [7–9] and amyloidogenic fibrils [10] is, however, still limited, which is in part due the low sensitivity and resolution being intrinsic to most solid-state NMR experiments.

In this study, we suggest the combined use of paramagnetic relaxation enhancement (PRE) and perdeuteration of proteins. The use of PRE for MAS solid-state NMR applications was pioneered by Ishii et al. [1,11–13]. In solution-state NMR, spin labels are used to provide restraints for structure determination [14,15]. In addition, they facilitate assignments in ligand binding experiments [16]. The use of spin labels has recently been successfully transferred to the solid-state [17]. The approach is expected to yield important restraints for the characterization of the quaternary structure in amyloidogenic peptides and proteins. Furthermore, it has been demonstrated that pseudocontact shifts in metalloproteins containing paramagnetic ions can provide important structural information for solid-state NMR structure calculations [18]. In case the interactions between the spin label and the molecule under investigation are unspecific, it has been shown that paramagnetic mole-

* Corresponding author. Address: Leibniz-Institut für Molekulare Pharmakologie (FMP), Robert-Rössle Str. 10, 13125 Berlin, Germany. Fax: +49 30 94793 199.
E-mail address: reif@fmp-berlin.de (B. Reif).

1090-7807/$ - see front matter © 2007 Elsevier Inc. All rights reserved.
doi:10.1016/j.jmr.2007.09.007

cules efficiently enhance the relaxation properties of a slowly relaxing solute spin [19,20]. Due to a shortening of the longitudinal T_1 relaxation time, a significant reduction of the experimental time can be achieved. At the same time, the T_2 relaxation time (and thus the line width) is merely affected [21–23].

Detection of protons in MAS solid-state NMR suffers from extreme line broadening induced by ^{1}H, ^{1}H homonuclear dipolar couplings, which are not effectively averaged out by the MAS spinning frequencies that are available to-date. Therefore, heteroatom detection schemes in combination with proton high power decoupling are applied to achieve high resolution in general. This conventional approach requires probe designs that are insensitive to high power RF irradiation. More important, the decoupling scheme induces a significant uptake of heat in the sample, in particular, if the sample contains high concentrations of ions (salt). For this reason, low-E probes have been developed to avoid problems associated with sample heating by partially excluding the electric field from the sample volume [24–26]. As a drawback, those probes commonly also have reduced B-fields, implying lower sensitivity. We demonstrated recently that direct proton detection can yield spectra with a resolution almost comparable to the resolution obtainable in solution-state NMR, in case protons are extensively diluted by deuterons [27,28]. Perdeuterated protein samples are re-crystallized from a buffer containing D_2O and H_2O using a mixing ratio of H_2O:D_2O = 1:9. Typically, amide proton resonance line widths in the order of 20-30 Hz are obtained this way in the direct dimension, setting the MAS rotation frequency to a value within 10-24 kHz. The scheme does not require high power proton decoupling in neither the nitrogen nor proton dimension. Only a very weak RF field in the order of 2.1 kHz is required to decouple the ^{1}H, ^{15}N scalar coupling. We and others could show previously, that deuteration and back-substitution of exchangeable protons allows for sensitive detection of protons [29–31], determination of long range ^{1}H, ^{1}H distances [32–34], and permits to localize mobile water molecules in the protein structure [35]. In addition, the ^{2}H spin can be used to probe side chain dynamics [36–39]. In contrast to the experimental scheme that was suggested by Ramamoorthy et al. [40], use of high power decoupling is redundant using the deuteration approach.

Spin dilution experiments suffer from the fact that 90% of the H_2O in the protein micro-crystals needs to be replaced with D_2O. The increase in resolution in the ^{1}H dimension results in a spectral quality which is comparable to solution-state NMR. As a drawback, however, only 10% of the exchangeable amide protons can contribute to the total signal intensity. On the other hand, MAS PRE experiments applied to protonated proteins might not be applicable if the investigated proteins are instable against RF induced heating. At the same time, short duty cycles can affect probe integrity as a result of high power decoupling. Application of PRE to proton diluted proteins allows to increase the signal-to-noise ratio per experimental time while maintaining the high resolution achieved by extensive deuteration of the protein. We show that the combination of perdeuteration and paramagnetic relaxation enhancement allows to overcome the limitations of each individual approach.

2. Materials and methods

2.1. Preparation of Cu–edta doped SH3 micro-crystals

SH3 protein was expressed in triply labeled M9 minimal media as described previously [6]. In addition to a stock solution of $(NH_4)_2SO_4$, a 350 mM $(NH_4)_2$[Cu(edta)]/$(NH_4)_2SO_4$ stock solution was prepared dissolving $CuSO_4$ (1.0 eq.) and H_4edta (1.05 eq.) in H_2O followed by adjustment of the pH to 5–6 using NH_4OH. For crystallization, a defined volume of a 12 mg/mL protein solution (pH 3.5) containing the desired amount of protein for crystallization was lyophilized. Similarly, a specific amount of the $(NH_4)_2SO_4$ stock was lyophilized for preparation of the copper-free samples. Dry protein and $(NH_4)_2SO_4$ powder were dissolved then in 10% H_2O, 90% D_2O, yielding a final concentration of 5 g/mL of protein and 150 mM of $(NH_4)_2SO_4$. For Cu^{II} containing samples, in addition to the protein a specific amount of the $(NH_4)_2$[Cu(edta)]/$(NH_4)_2SO_4$ stock solution was lyophilized to yield the indicated chelate complex concentration in the crystallization batch later. To ensure a certain minimum ionic strength required for crystallization (corresponding to the original 150 mM $[X^+]_2[Y^-]$), the respective amount of the $(NH_4)_2SO_4$ stock solution was additionally lyophilized for the preparation of the 10 mM $[Cu(edta)]^{2-}$ sample. After dissolving all components in the H_2O/D_2O mixture, the pH of the solution was shifted from 3.5 to 7.5–8.0 by addition of NH_3. In the low concentrated Cu–edta samples, the amount of NH_3 needed for the pH shift was very small. To adjust the pH, a few microliter of a dilute NH_4OH solution were added. The pH was verified using pH paper. Larger amounts of NH_3 were necessary for the preparation of the 250 mM sample. Therefore, gaseous NH_3 was bubbled through the solution using a Eppendorf pipette in order not to dilute the protein and the Cu–edta solution. Several minutes after shifting the pH, crystals started to form as judged by the turbidity of the solution. After complete precipitation at 4 °C overnight, the micro-crystals were spun into a 3.2-mm rotor and the residual supernatant was carefully taken off. For each sample, 2–6 mg of protein was packed into the NMR rotor.

2.2. NMR spectroscopy

Protein spectra were recorded at a magnetic field strength of 16.4 T, corresponding to a proton Larmor frequency of 700 MHz. All experiments were carried out using a Bruker AV700WB spectrometer, equipped with a stan-

dard 3.2 mm triple-resonance probe. ^{1}H, ^{15}N correlation experiments were recorded adjusting the MAS rotation frequency to 24 kHz spinning and maintaining the nominal temperature at 275 K. Proton 1D NMR spectra were recorded using an ^{15}N x-filter including a delay for water dephasing of 8 ms (Fig. 1c). Data were acquired for a period of 80 ms. The experimental spectra were processed without use of window functions in the acquisition dimension. 2D ^{1}H, ^{15}N correlation spectra were recorded omitting the 180° inversion pulse at the beginning of the pulse sequence. Each 2D was recorded acquiring 160 data points in the indirect dimension. For the ^{15}N evolution period, a dwell time of 250 μs was used, yielding $t_1^{max} = 40$ ms (140 data points corresponding to 35 ms for the 250 mM Cu–edta sample). An acquisition time in the proton dimension of 80 ms was used. Procession was performed applying a cosine squared apodization function prior to Fourier transformation in both dimensions. ^{1}H T_1 data were recorded using the 1D inversion recovery experiments shown in Fig. 1c. Ten data points of different inversion times Δ were recorded for each sample. For this measurement, the recycle delay was set to 15 s, 8 s, 10 s and 3 s for samples containing 0 mM, 10 mM, 75 mM and 250 mM $[Cu^{II}(edta)]^{2-}$, respectively.

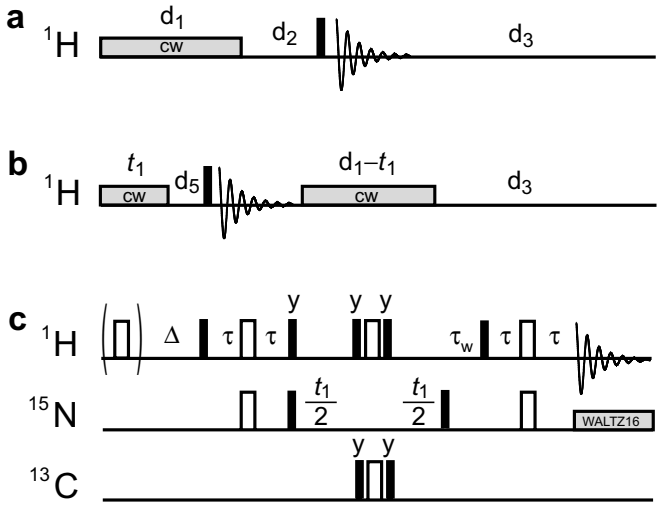

Fig. 1. Pulse sequence schemes to estimate the temperature increase of H_2O induced by high power RF irradiation on the ^{1}H channel. (a) Determination of the steady-state temperature increase. RF is irradiated during a constant time d_1 (30 ms). d_2 is typically set to 30 ms to allow for an equilibration of the system. d_3 is adjusted to $(d_3 = RD - \sum d_i - aq.)$, where RD refers to the recycle delay of the experiment (aq = 200 ms). The flow-rate of the cooling gas was adjusted to 1335 L/h. Black bars indicate 90° pulses. (b) Determination of the dynamic temperature increase during decoupling. The delay t_1 is systematically incremented from 0 to d_1. At the same time, the second block of decoupling is decremented from d_1 to 0. d_5 is set to 1 ms. (c) ^{1}H T_1 measurement and ^{1}H, ^{15}N correlation experiments. For magnetization transfer, a double INEPT pulse sequence element was employed. The MAS rotation frequency was adjusted to $\nu_r = 24$ kHz. For the inversion recovery experiments, incrementation of t_1 was omitted, whereas for ^{1}H, ^{15}N correlation experiments, the inversion pulse was left out. The delays $\tau = 2.17$ ms and $\tau_w = 8$ ms were employed.

3. Results and discussion

In this study, we demonstrate that sensitivity enhancement experiments using complexed paramagnetic ions are greatly facilitated in the solid-state if perdeuterated proteins are employed. The results section is therefore split into two parts:

The first part describes quantitative measurements of the heating effects which are induced in salt-free and salt-containing water samples by application of high power RF decoupling. The experiments are carried out using a standard Bruker 3.2 mm probe. It is obvious that probes for which the electric field is excluded from the active sample volume will show reduced uptake of heat [24–26]. Probe design, however, cannot be the final solution to this problem, keeping in mind that the resolution obtained in, e.g. the ^{15}N dimension using the deuteration scheme described above, requires acquisition times of up to 100 ms. At the same time, we aim at reducing the recycle delay of the experiment to a few hundred milliseconds using PRE.

In the second part, we demonstrate that the combination of PRE and the use of perdeuterated proteins indeed results in high resolution MAS solid-state NMR spectra. The use of complexed paramagnetic ions does not compromise resolution even at the highest concentration (250 mM Cu–edta).

3.1. Heating of the sample induced by high power RF irradiation

Heating effects induced by proton decoupling were investigated employing water samples containing 0 mM and 100 mM NaCl. The water resonance frequency is very sensitive to temperature and can therefore be used as an internal sample thermometer [41,42]. For calibration purposes, the water chemical shift was first monitored in the temperature range of 275–335 K, setting the MAS frequency to a low value ($\nu_r = 1600$ Hz). The system was allowed to equilibrate for 15 min before each temperature point was recorded (see Supporting information).

In order to study the effects of RF irradiation on the sample temperature, the temperature controller was set to a temperature of 275 K. The flow-rate of the cooling gas was adjusted to 1335 L/h in order to assess the steady-state temperature increase, whereas it was set to 935 L/h and 1335 L/h to measure the dynamic increase of the temperature of the salt-containing and the salt-free water sample, respectively, within the acquisition time. CW irradiation was off-set from the carrier frequency by 100 kHz to prevent saturation of the water resonance. Dummy scans were carried out for 10 min to equilibrate the system before the actual experiment was recorded and the FID was saved.

The dependence of the steady-state temperature increase is represented in Fig. 2 as a function of the inverse recycle delay, the ^{1}H decoupling power and the salt concentration using the pulse scheme represented in Fig. 1a.

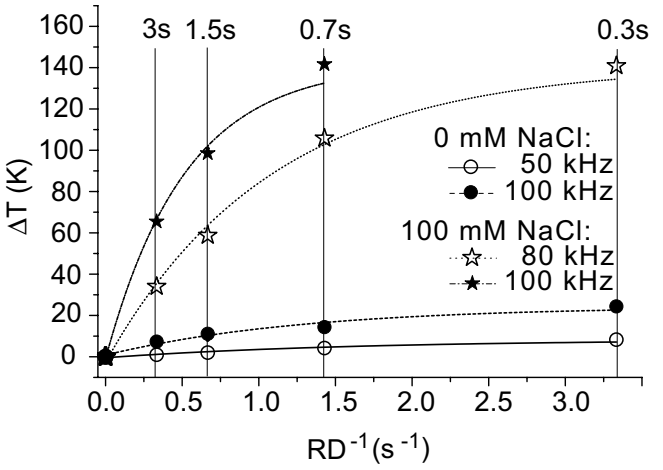

Fig. 2. Temperature increases in a 3.2-mm MAS rotor (30 μL) due to high power ^{1}H decoupling, as a function of the inverse (RD^{-1}) of the recycle delay RD, which is indicated on top of the figure. d_1 is set to 30 ms in this experiment. Circles and stars indicate experiments carried out on a H_2O sample containing no and 100 mM NaCl, respectively. Open and closed symbols show the effect of heating upon change of the RF decoupling field.

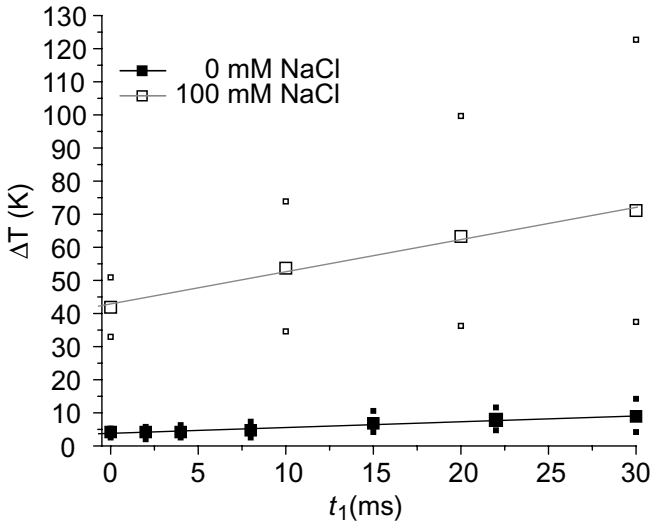

Fig. 3. Dynamic temperature increases in a 3.2-mm MAS rotor (30 μL) after a variable length of decoupling ranging from 0 to 30 ms, corresponding to the pulse scheme indicated in Fig. 1b. Data were recorded for a sample containing no salt (closed symbols) and 100 mM NaCl (open symbols). Major symbols represent the center of the integral, whereas minor symbols reflect the chemical shift, and thus the temperature, at ±37.5% of the total integral around the average chemical shift. The spectrum was acquired 1 ms after the off-resonance decoupling. A recycle delay of 3 s, a decoupling RF field strength of 100 kHz and a flow-rate of the cooling gas of 935 L/h were employed in all experiments.

The measured temperature increases of the no salt-containing water sample is still moderate and amounts to approximately 24 K (8 K) after an RF irradiation of 30 ms using an RF field strength of 100 kHz (50 kHz) and a relatively short recycle delay of 0.3 s. Due to the increased susceptibility in the salt-containing sample, energy uptake is considerably higher. The temperature in the sample rises by about 100 K and more directly after decoupling. Recycle delays for experiments using 100 kHz decoupling were chosen longer than 0.7 s in order to avoid sample burst. The value of the precise sample temperature may deviate due to the limited temperature range chosen for calibration (0–60 °C) and the assumption of a perfect linearity, which is not valid anymore at temperatures close to the boiling point of water [41].

In order to appreciate the dynamic temperature increase induced in the sample in the course of a decoupling sequence, acquisition was sandwiched in two blocks of decoupling, while the integral decoupling time is kept constant (Fig. 1b). The length of the RF irradiation was systematically increased before acquisition of the water signal. Simultaneously, the decoupling period after acquisition was decremented to ensure that the applied power over one cycle was constant upon incrementation of t_1.

A 100 kHz CW RF field was applied in all experiments. While an increase of only 5 K is observed for the salt-free sample (cooling gas flow-rate 1335 L/h), the temperature for the sample containing 100 mM NaCl rises to approximately 30 K above the minimum value within one cycle (cooling gas flow-rate 935 L/h) (Fig. 3). Non-zero slopes indicate that the sample would experience different temperatures during the acquisition of data points in either the direct or indirect evolution period. This temperature increase cannot be avoided, not even if infinitely long recycle delays could be employed. In Fig. 3, the center of gravity of the integral of the resulting water signal is depicted. Small symbols reflect the water chemical shift value, and thus the temperature, at ±37% of the total integral around the average water chemical shift. Especially at high power RF irradiation, a wide distribution of water chemical shifts are observed, which might be due to a temperature gradient across the sample.

3.2. PRE experiments in perdeuterated proteins

As a model protein for solid-state NMR spectroscopic investigations, we use the SH3 domain from chicken α-spectrin. In order to investigate the behaviour upon addition of chelated paramagnetic ions, the protein was crystallized in the presence of different concentrations of $(NH_4)_2$[Cu(edta)]. Upon addition of $[Cu(edta)]^{2-}$, no changes of the macroscopic micro-crystalline structure could be detected by light microscopy. The comparison of the NMR data recorded with samples of different amounts of copper reveals a strong reduction of the T_1 relaxation time. The bulk amide proton intensities were fit using a mono-exponential fit function. The respective curves together with the extracted T_1 relaxation rates are shown in Fig. 4.

The reference sample, which does not contain the Cu–edta chelate complex, yields a longitudinal relaxation time T_1 in the order of (4.4 ± 0.2) s. This T_1 value is rather long compared to the relaxation time of a protonated sample (approximately 1 s). This is due to the high degree of pro-

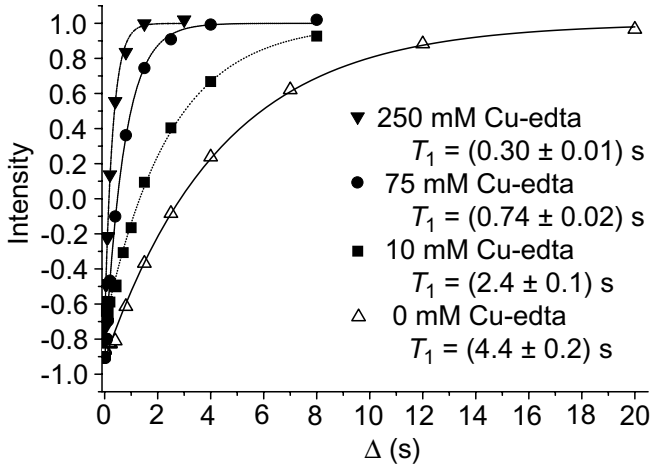

Fig. 4. Inversion recovery curves of the amide protons in the SH3 domain of α-spectrin employing 0, 10, 75 and 250 mM Cu^{II}. The longitudinal relaxation time decreased from 4.4 to 2.4, 0.7 and 0.3 s. T_1 was determined by integration of the bulk amid proton signals. The recycle delays in the experiments were set to 15 s (no $[Cu(edta)]^{2-}$), 8 s (10 mM), 10 s (75 mM) and 3 s (250 mM).

ton dilution. In the deuterated sample, ^1H, ^1H dipolar couplings are reduced significantly, which is required to achieve high resolution in the ^1H dimension. By adding 10 mM, 75 mM and 250 mM Cu–edta to the protein sample, a relaxation enhancement of a factor of 1.8 ($T_1 = (2.4 \pm 0.1)$ s), 6.0 ($T_1 = (0.74 \pm 0.02)$ s) and 15 $T_1 = (0.30 \pm 0.01)$ s, could be achieved. As no high power decoupling is required using the deuteration scheme, the recycle delay can be reduced by the same factor. The time required to record a high-resolution proton detected correlation spectrum thus decreases significantly.

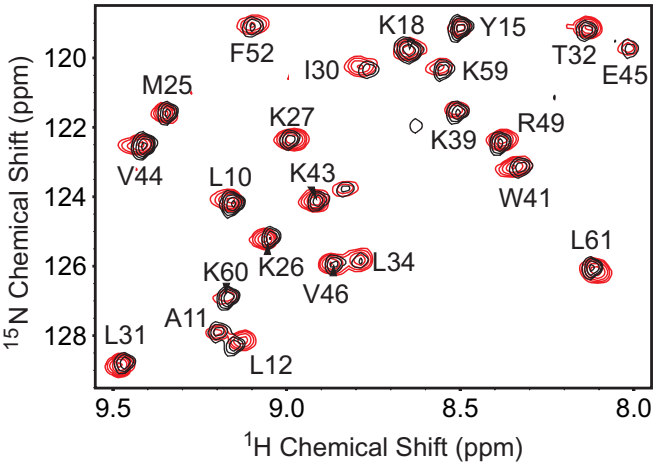

Fig. 5. Superposition of a ^1H detected ^1H, ^{15}N correlation experiment in the absence (black) and presence of 250 mM $[Cu(edta)]^{2-}$ (red). The figure represents only a part of the total spectrum. In general, only negligible chemical shift changes are observed upon addition of Cu–edta (see also Fig. 8a). In the experiment, the MAS rotation frequency was set to 24 kHz. The effective temperature of the sample amounted to approximately 295 K.

No significant chemical shift changes could be observed upon addition of Cu–edta (Fig. 5). Thus, a specific binding of the chelated complex to specific protein residues, as presumed earlier [23], could not be found. The line widths of protons as well as for nitrogen resonances are not compromised by the chelate at a concentration of 75 mM. Only a slight broadening effect of around 7 Hz is observed at a complex concentration of 250 mM (see below). Fig. 6 represents nitrogen filtered ^1H spectra of the SH3 domain of samples containing 0, 75 and 250 mM copper.

Samples with different concentrations of Cu–edta contained different amounts of protein. Therefore, the signal-to-noise ratio is slightly different in the three experiments. Fig. 7 represents the projection along the ^{15}N axis of the ^1H, ^{15}N correlation experiments using different Cu–edta concentrations. The single resonance on the right side of the figure displays the amide resonance of L31, which was extracted from the 2D ^1H, ^{15}N correlation experiments as a column vector. All spectra were processed without

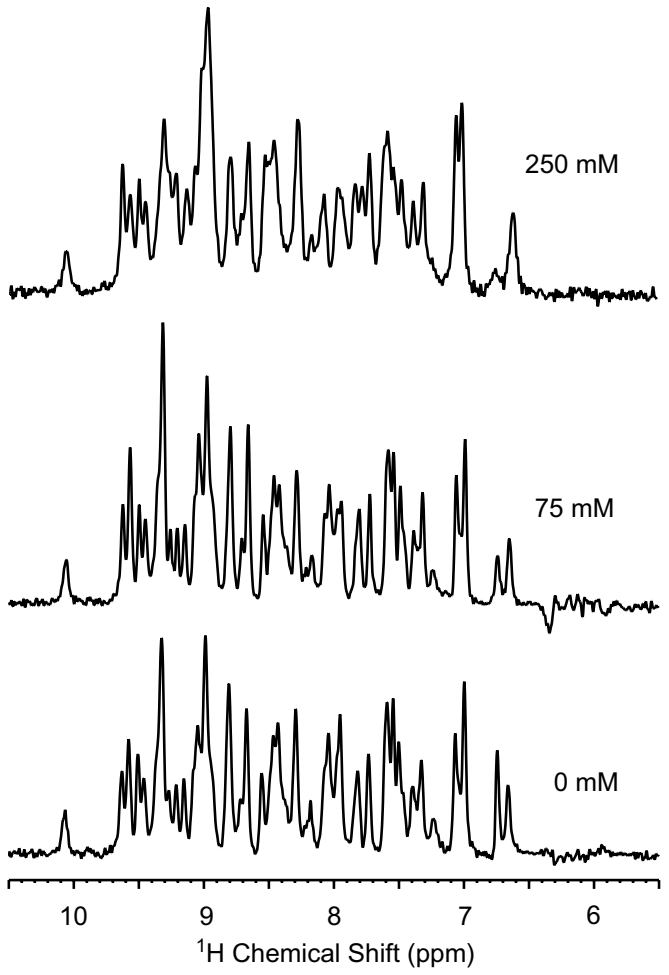

Fig. 6. Comparison of the H^N resonances as a function of the Cu–edta concentration. The high resolution due to the low level of protonation is not lost after addition of $[Cu(edta)]^{2-}$. Spectra were processed without apodization.

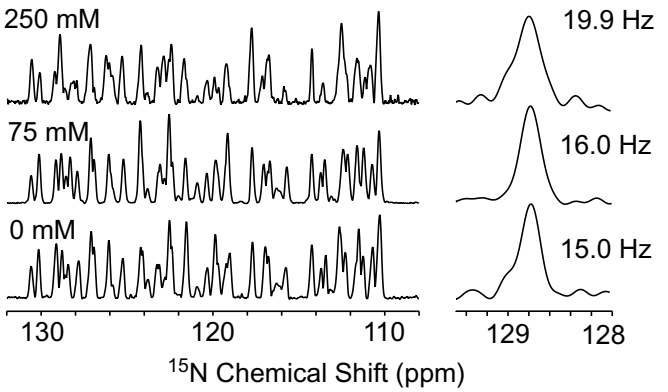

Fig. 7. ^{15}N line widths of Cu–edta doped micro-crystalline SH3 samples. Projection along the ^{15}N dimension of the 2D ^{1}H, ^{15}N correlation (left). Columns extracted from the 2D HSQC across the correlation signal corresponding to L31 along the ^{15}N dimension (right). All experiments were recorded to yield t_1^{max} (^{15}N) = 70 ms.

apodization in the ^{15}N dimension. The ^{15}N line widths were determined to be 15.0 Hz, 16.0 Hz and 19.9 Hz (FWHM) for samples containing 0 mM, 75 mM and 250 mM $[Cu^{II}(edta)]^{2-}$, respectively.

A more detailed analysis of the effect that Cu–edta has on the ^{1}H line width and the isotropic chemical shift difference is given in Fig. 8. Fig. 8a represents the ^{1}H line width of each residue (FWHM) as a function of the amino acid sequence. We find that the average proton natural line width amounts to (24.3 ± 5.5) Hz and (31.5 ± 7.5) Hz for samples containing 75 mM and 250 mM Cu–edta, respectively. In contrast, the ^{1}H line width of the reference sample was determined to be (24.6 ± 5.3) Hz. This indicates that Cu–edta concentrations up to 75 mM leave the proton line width unaffected, whereas the higher concentration of 250 mM Cu–edta induces a modest increase of approximately 7 Hz of the ^{1}H line width.

Similarly, we find that the isotropic chemical shifts of ^{1}H and ^{15}N are not significantly affected, even at a Cu–edta concentration of 250 mM (Fig. 8b). For the superposition of two spectra, the RMS difference of the chemical shift differences was minimized. In the figure, the chemical shift difference $\Delta\delta = \{[\Delta\delta(^{1}H)]^2 + [\Delta\delta(^{15}N)]^2\}^{1/2}$ (all values in Hertz) of samples with and without copper is represented as a function of the primary sequence. At a concentration of 250 mM Cu–edta, the average change in peak position amounts to (8.7 ± 7.1) Hz which is within the natural line width of the ^{15}N and ^{1}H resonances.

4. Conclusion

We show that the feasibility of paramagnetic relaxation enhancement experiments using chelated paramagnetic complexes in MAS solid-state NMR can be substantially improved if experiments are carried out using perdeuterated proteins in which labile protons are back-exchanged from H_2O/D_2O containing buffer solutions. In conventional solid-state NMR experiments, the short duty cycle induces a significant uptake of heat in the sample even for short acquisition times, as high power proton decoupling is most often obligatory. At the same time, short duty cycles can affect probe integrity. The potency of PRE can be exploited at best for samples in which the proton spin system is strongly chemically diluted. At the same time, the reduction of sensitivity implied by the labeling scheme can be almost compensated. Compared to the non-doped protein preparation, we gain a reduction in measurement time of up to a factor of 15. Chemical shifts are not significantly affected upon addition of the chelated paramagnetic complex. The resolution in both the ^{1}H and ^{15}N dimension is not compromised. The increase in line width (^{1}H/^{15}N) is in the order of a few Hertz in all cases.

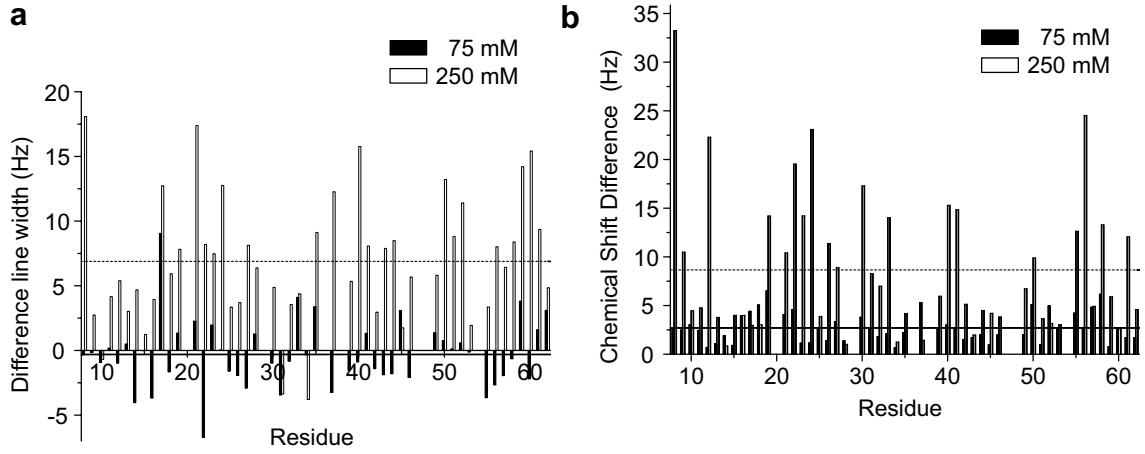

Fig. 8. (a) Differences in ^{1}H line widths obtained for a 75 mM (closed rectangles) and 250 mM (open rectangles) Cu–edta doped SH3 sample, compared to a copper-free reference sample as a function of the amino acid sequence. Horizontal solid and dashed lines in the figure indicate the average value of the line width difference for samples containing 75 mM and 250 mM Cu–edta, respectively. (b) Chemical shift differences of the samples containing 75 mM (closed rectangles) and 250 mM $[Cu(edta)]^{2-}$ (open rectangles) with respect to a sample containing no copper. Horizontal solid and dashed lines in the figure indicate the average value of the chemical shift difference for samples containing 75 mM and 250 mM Cu–edta, respectively.

Acknowledgments

We thank Kristina Rehbein for providing the triply labeled protein. The authors are grateful to Prof. Hartmut Oschkinat for continuous support of this project. We thank Tomas Jacso, Katja Faelber, Mangesh Joshi, Vipin Agarval, Muralidhar Dasari, and Uwe Fink for a lot of help and stimulating discussion. R.L. is a Kekulé scholar and acknowledges support from the Verband der Chemischen Industrie. This research was supported by the DFG Grant Re1435.

Appendix A. Supplementary data

Supplementary data associated with this article can be found, in the online version, at doi:10.1016/j.jmr.2007.09.007.

References

[1] N.P. Wickramasinghe, M. Kotecha, A. Samoson, J. Past, Y. Ishii, Sensitivity enhancement in C-13 solid-state NMR of protein microcrystals by use of paramagnetic metal ions for optimizing H-1 T-1 relaxation, J. Magn. Reson. 184 (2007) 350–356.

[2] F. Castellani, B.-J. van Rossum, A. Diehl, M. Schubert, K. Rehbein, H. Oschkinat, Structure of a protein determined by solid-state magic-angle spinning NMR, Nature 420 (2002) 98–102.

[3] S.G. Zech, A.J. Wand, A.E. McDermott, Protein structure determination by high-resolution solid-state NMR spectroscopy: Application to microcrystalline ubiquitin, J. Am. Chem. Soc. 127 (2005) 8618–8626.

[4] N. Giraud, A. Böckmann, A. Lesage, F. Penin, M. Blackledge, L. Emsley, Site-specific backbone dynamics from a crystalline protein by solid-state NMR spectroscopy, J. Am. Chem. Soc. 126 (2004) 11422–11423.

[5] J.L. Lorieau, A.E. McDermott, Conformational flexibility of a microcrystalline globular protein: Order parameters by solid-state NMR spectroscopy, J. Am. Chem. Soc. 128 (2006) 11505–11512.

[6] V. Chevelkov, K. Faelber, A. Schrey, K. Rehbein, A. Diehl, B. Reif, Differential line broadening in MAS solid-state NMR due to dynamic interference, J. Am. Chem. Soc. 129 (2007) 10195–10200.

[7] O.C. Andronesi, S. Becker, K. Seidel, H. Heise, H.S. Young, M. Baldus, Determination of membrane protein structure and dynamics by magic-angle-spinning solid-state NMR spectroscopy, J. Am. Chem. Soc. 127 (2005) 12965–12974.

[8] M. Hiller, L. Krabben, K.R. Vinothkumar, F. Castellani, B. Van Rossum, W. Kühlbrandt, H. Oschkinat, Solid-state magic-angle spinning NMR of outer-membrane protein G from *Escherichia coli*, Chem. Bio. Chem. 6 (2005) 1679–1684.

[9] A. Lange, K. Giller, S. Hornig, M.F. Martin-Eauclaire, O. Pongs, S. Becker, M. Baldus, Toxin-induced conformational changes in a potassium channel revealed by solid-state NMR, Nature 440 (2006) 959–962.

[10] A.B. Siemer, C. Ritter, M. Ernst, R. Riek, B.H. Meier, High-resolution solid-state NMR spectroscopy of the prion protein HET-s in its amyloid conformation, Angew. Chem. Int. Ed. 44 (2005) 2441–2444.

[11] Y. Ishii, N.P. Wickramasinghe, S. Chimon, A new approach in 1D and 2D C-13 high-resolution solid-state NMR spectroscopy of paramagnetic organometallic complexes by very fast magic-angle spinning, J. Am. Chem. Soc. 125 (2003) 3438–3439.

[12] N.P. Wickramasinghe, M. Shaibat, Y. Ishii, Enhanced sensitivity and resolution in H-1 solid-state NMR spectroscopy of paramagnetic complexes under very fast magic angle spinning, J. Am. Chem. Soc. 127 (2005) 5796–5797.

[13] N.P. Wickramasinghe, Y. Ishii, Sensitivity enhancement, assignment, and distance measurement in C-13 solid-state NMR spectroscopy for paramagnetic systems under fast magic angle spinning, J. Magn. Reson. 181 (2006) 233–243.

[14] J.R.S.D. Gillespie, Characterization of long-range structure in the denatured state of staphylococcal nuclease.1. Paramagnetic relaxation enhancement by nitroxide spin labels, J. Mol. Biol. 268 (1997) 158–169.

[15] J.L. Battiste, G. Wagner, Utilization of site-directed spin labeling and high-resolution heteronuclear nuclear magnetic resonance for global fold determination of large Proteins with limited Nuclear Overhauser effect data, Biochem. 39 (2000) 5355–5365.

[16] B. Cutting, A. Strauss, G. Fendrich, P.W. Manley, W. Jahnke, NMR resonance assignment of selectively labeled proteins by the use of paramagnetic ligands, J. Biomol. NMR 30 (2004) 205–210.

[17] P.S. Nadaud, J.J. Helmus, N. Höfer, C.P. Jaroniec, Long-range structural restraints in spin-labeled proteins probed by solid-state nuclear magnetic resonance spectroscopy, J. Am. Chem. Soc. 129 (2007) 7502–7503.

[18] S. Balayssac, I. Bertini, M. Lelli, C. Luchinat, M. Maletta, Paramagnetic ions provide structural restraints in solid-state NMR of proteins, J. Am. Chem. Soc. 129 (2007) 2218–2219.

[19] I. Solomon, Relaxation processes in a system of two spins, Phys. Rev. 99 (1955) 559–565.

[20] P. Luginbuhl, K. Wuthrich, Semi-classical nuclear spin relaxation theory revisited for use with biological macromolecules, Prog. NMR Spect. 40 (2002) 199–247.

[21] J.L. Barnhart, R.N. Berk, Influence of paramagnetic ions and pH on proton NMR relaxation of biological fluids, Invest. Radiol. 21 (1986) 132–136.

[22] C. Luchinat, Z.C. Xia, Paramagnetism and dynamic properties of electrons and nuclei, Coord. Chem. Rev. 120 (1992) 281–307.

[23] S. Cai, C. Seu, Z. Kovacs, A.D. Sherry, Y. Chen, Sensitivity enhancement of multidimensional NMR experiments by paramagnetic relaxation effects, J. Am. Chem. Soc. 128 (2006) 13474–13478.

[24] J.A. Stringer, C.E. Bronnimann, C.G. Mullen, D.H.H. Zhou, S.A. Stellfox, Y. Li, E.H. Williams, C.M. Rienstra, Reduction of RF-induced sample heating with a scroll coil resonator structure for solid-state NMR probes, J. Magn. Res. 173 (2005) 40–48.

[25] F.D. Doty, J. Kulkarni, C. Turner, G. Entzminger, A. Bielecki, Using a cross-coil to reduce RF heating by an order of magnitude in triple-resonance multinuclear MAS at high fields, J. Magn. Reson. 182 (2006) 239–253.

[26] P.L. Gor'kov, E.Y. Chekmenev, C. Li, M. Cotten, J.J. Buffy, N.J. Traaseth, G. Veglia, W.W. Brey, Using low-E resonators to reduce RF heating in biological samples for static solid-state NMR up to 900 MHz, J. Magn. Reson. 185 (2007) 77–93.

[27] V. Chevelkov, K. Rehbein, A. Diehl, B. Reif, Ultra-high resolution in proton solid-state NMR at high levels of deuteration, Angew. Chem. Int. Ed. 45 (2006) 3878–3881.

[28] V. Agarwal, A. Diehl, N. Skrynnikov, B. Reif, High Resolution 1H Detected 1H,13C Correlation spectra in MAS solid-state NMR using deuterated proteins with selective 1H,2H isotopic labeling of methyl groups, J. Am. Chem. Soc. 128 (2006) 12620–12621.

[29] B. Reif, R.G. Griffin, ^{1}H detected ^{1}H, ^{15}N correlation spectroscopy in rotating solids, J. Magn. Reson. 160 (2003) 78–83.

[30] V. Chevelkov, B.J.v. Rossum, F. Castellani, K. Rehbein, A. Diehl, M. Hohwy, S. Steuernagel, F. Engelke, H. Oschkinat, B. Reif, 1H detection in MAS solid state NMR spectroscopy employing pulsed field gradients for residual solvent suppression, J. Am. Chem. Soc. 125 (2003) 7788–7789.

[31] E.K. Paulson, C.R. Morcombe, V. Gaponenko, B. Dancheck, R.A. Byrd, K.W. Zilm, Sensitive high resolution inverse detection NMR spectroscopy of proteins in the solid state, J. Am. Chem. Soc. 125 (2003) 15831–15836.

[32] B. Reif, C.P. Jaroniec, C.M. Rienstra, M. Hohwy, R.G. Griffin, ^{1}H-^{1}H MAS correlation spectroscopy and distance measurements in a deuterated peptide, J. Magn. Reson. 151 (2001) 320–327.
[33] B. Reif, B.J. van Rossum, F. Castellani, K. Rehbein, A. Diehl, H. Oschkinat, Determination of ^{1}H ^{1}H distances in a uniformly ^{2}H, ^{15}N labeled SH3 domain by MAS solid state NMR spectroscopy, J. Am. Chem. Soc. 125 (2003) 1488–1489.
[34] E.K. Paulson, C.R. Morcombe, V. Gaponenko, B. Dancheck, R.A. Byrd, K.W. Zilm, High-sensitivity observation of dipolar exchange and NOEs between exchangeable protons in proteins by 3D solid-state NMR spectroscopy, J. Am. Chem. Soc. 125 (2003) 14222–14223.
[35] V. Chevelkov, K. Faelber, A. Diehl, U. Heinemann, H. Oschkinat, B. Reif, Detection of dynamic water molecules in a microcrystalline sample of the SH3 domain of α-spectrin by MAS solid-state NMR, J. Biomol. NMR 31 (2005) 295–310.
[36] M. Hologne, K. Faelber, A. Diehl, B. Reif, Characterization of dynamics of perdeuterated proteins by MAS solid-state NMR, J. Am. Chem. Soc. 127 (2005) 11208–11209.
[37] M. Hologne, Z. Chen, B. Reif, Characterization of dynamic processes using deuterium in uniformly 2H,13C,15N enriched peptides by MAS solid-state NMR, J. Magn. Res. 179 (2006) 20–28.
[38] B. Reif, Y. Xue, V. Agarwal, M.S. Pavlova, M. Hologne, A. Diehl, Y.E. Ryabov, N.R. Skrynnikov, Protein side-chain dynamics observed by solution- and solid-state NMR: Comparative analysis of methyl ^{2}H relaxation data, J. Am. Chem. Soc. 128 (2006) 12354–12355.
[39] M. Hologne, V. Chevelkov, B. Reif, Deuteration of peptides and proteins in MAS solid-state NMR, Prog. NMR Spect. 48 (2006) 211–232.
[40] S.V. Dvinskikh, K. Yamamoto, U.H.N. Durr, A. Ramamoorthy, Sensitivity and resolution enhancement in solid-state NMR spectroscopy of bicelles, J. Magn. Reson. 184 (2007) 228–235.
[41] J.C. Hindman, Proton resonance shift of water in gas and liquid states, J. Chem. Phys. 44 (1966) 4582–4583.
[42] S.V. Dvinskikh, V. Castro, D. Sandstrom, Heating caused by radiofrequency irradiation and sample rotation in C-13 magic angle spinning NMR studies of lipid membranes, Magn. Res. Chem. 42 (2004) 875–881.